Physica Scripta

PAPER

Dynamical analysis of higher-order localized waves for a three-component coupled nonlinear Schrödinger equation

N Song[1,*], Y F Zhang[1], H J Shang[1] and W X Ma[2,3,4,5,*]

[1] School of Mathematics, North University of China, Taiyuan, Shanxi, 030051, People's Republic of China
[2] Department of Mathematics, Zhejiang Normal University, Jinhua, Zhejiang, 321004, People's Republic of China
[3] Department of Mathematics, King Abdulaziz University, Jeddah 21589, Saudi Arabia
[4] Department of Mathematics and Statistics, University of South Florida, Tampa, FL 33620-5700, United States of America
[5] School of Mathematical and Statistical Sciences, North-West University, Mafikeng Campus, Private Bag X2046, Mmabatho 2735, South Africa
[*] Authors to whom any correspondence should be addressed.

E-mail: songni@nuc.edu.cn **and** mawx@cas.usf.edu

RECEIVED
27 September 2022

REVISED
15 January 2023

ACCEPTED FOR PUBLICATION
31 January 2023

PUBLISHED
13 February 2023

Keywords: three-component coupled Schrödinger equation, generalized Darboux transformation, localized waves, rogue waves

Abstract

This paper examines the three-component coupled nonlinear Schrödinger equation, which has various applications in deep ocean, nonlinear optics, Bose–Einstein (BE) condensates, and more. On the basis of seed solutions and a Lax pair, the Nth-order iterative expressions for the solutions are derived by using the generalized Darboux transformation. The evolution plots of dark-bright-rogue wave or breather-rogue wave are then obtained via numerical simulation. Particularly, a novel rogue wave propagation trajectory is found in the second and third order localized wave solutions. Moreover, by increasing the value of the free parameter α and β, the nonlinear waves merge with each other distinctly. The results further reveal the abundant dynamical patterns of localized waves in the three-component coupled system.

1. Introduction

The Multi-component coupled nonlinear Schrödinger (NLS) equations can be used to describe a variety of complex physical phenomena, and they possess more abundant dynamical behaviors of localized wave solutions than do the scalar NLS equations [1–7]. Rogue waves on a multi-soliton background for the Manakov system have been studied by using the Darboux-dressing transformation [1]. The bright–dark–rogue solution [2] and other higher-order localized waves are all found in a two-component coupled NLS equation [3, 4]. A four-petaled flower structure rogue wave is exhibited in a three-component coupled NLS equation [5]. Soliton solutions are generated from the binary Darboux transformation (DT) for multicomponent NLS equations and their reductions [6]. The general N-soliton solution and Nth-order vector rational and semi-rational rogue waves for a three-component coupled NLS equation have also been found by using different methods [7, 8]. Meanwhile, many methods have been presented to find localized wave solutions, including Bäcklund transformation [9–11], the nonlinear steepest descent method [11–15], the Riemann–Hilbert approach [16], the DT [17–20], and more. Based on the profound theoretical significance and potential applicability, the study of localized waves of the multi-component NLS equations has always been important, and great progresses have been made [21–24] in this area.

Motivated by the aforesaid work, the three-component coupled NLS equation is considered [27–30]:

$$\begin{aligned} &iq_{1t} + \frac{1}{2}q_{1xx} + \sigma(|q_1|^2 + |q_2|^2 + |q_3|^2)q_1 = 0, \\ &iq_{2t} + \frac{1}{2}q_{2xx} + \sigma(|q_1|^2 + |q_2|^2 + |q_3|^2)q_2 = 0, \end{aligned} \tag{1}$$

$$iq_{3t} + \frac{1}{2}q_{3xx} + \sigma(|q_1|^2 + |q_2|^2 + |q_3|^2)q_3 = 0,$$

which can be applied in plasma physics [25], nonlinear optics [26], Bose–Einstein condensates [27], and some others. Vijayajayanthi *et al* derived the vector soliton solution of equation (1) by the Horita bilinear method [28]. Based on the generalized DT, Zhang *et al* gave the expression of the *N*th-order vector rational and semi-rational rogue solutions of equation (1) [29]. For the convenience of calculation, σ is taken as 1. Wang *et al* displayed the new breather wave and rogue wave solutions for equation (1) at $\sigma = 1$ by using the DT [30]. Peng *et al* obtained multi-soliton solutions for equation (1) at $\sigma = 1$ via the Riemann–Hilbert method [31]. However, there are fewer studies on the dynamics of higher-order localized waves for equation (1) at $\sigma = 1$. In this paper, a generalized DT is used to study the equation (1), and a novel propagation trajectory of higher-order rogue waves is obtained.

The remainder of this paper is organized as follows. In section 2, a generalized DT for equation (1) is constructed, and the iterative formulas of the *N*th-order solutions are derived. In section 3, the higher-order rogue waves on a multi-bright-dark soliton or multi-breathers are derived, and some evolution plots of localized wave solitons are illustrated. Finally, several conclusions are drawn in section 4.

2. Generalized darboux transformation

The Lax pair corresponding to equation (1) at $\sigma = 1$ is

$$\Phi_x = U\Phi = (i\lambda\Lambda + Q)\Phi \tag{2a}$$

$$\Phi_t = V\Phi = \left(i\lambda^2 + \lambda Q + \frac{1}{2}i\Lambda(Q^2 - Q_x)\right)\Phi \tag{2b}$$

where

$$Q = \begin{pmatrix} 0 & -q_1^* & -q_2^* & -q_3^* \\ q_1 & 0 & 0 & 0 \\ q_2 & 0 & 0 & 0 \\ q_3 & 0 & 0 & 0 \end{pmatrix}, \quad \Lambda = diag\,(1, -1, -1, -1)$$

$\Phi = (\varphi, \phi, \psi, \chi)^T$ is a vector solution of equation (2), λ is the spectral parameter, $q_i (i = 1, 2, 3)$ is the potential function, and $*$ represents the complex conjugate. Thus, it can be easily proven that the zero-curvature equation, $U_t - V_x + [U, V] = 0$, yields in equation (1).

The Darboux matrix is constructed as follows:

$$T = \lambda I - H\Lambda H^{-1} \tag{3}$$

where

$$\Lambda = \begin{pmatrix} \lambda_1 & 0 & 0 & 0 \\ 0 & \lambda_1^* & 0 & 0 \\ 0 & 0 & \lambda_1^* & 0 \\ 0 & 0 & 0 & \lambda_1^* \end{pmatrix}, \quad H = \begin{pmatrix} \varphi_1 & \phi_1^* & \psi_1^* & \chi_1^* \\ \phi_1 & -\varphi_1^* & 0 & 0 \\ \psi_1 & 0 & -\varphi_1^* & 0 \\ \chi_1 & 0 & 0 & -\varphi_1^* \end{pmatrix}$$

I is the identity matrix, and $\Phi_k = (\varphi_k, \phi_k, \psi_k, \chi_k)^T \ (k = 1, 2, \cdots)$ is the solution to equation (2) for $\lambda = \lambda_k$. The classical DT definition is as follows:

$$\Phi_N[N-1] = T[N-1]T[N-2]\cdots T[1]\Phi_N, \tag{4}$$

$$q_1[N] = q_1[0] - 2i\sum_{k=1}^{N}(\lambda_k - \lambda_k^*)\frac{\varphi_k^*[k-1]\phi_k[k-1]}{|\phi_k[k-1]|^2 + |\varphi_k[k-1]|^2 + |\chi_k[k-1]|^2 + |\psi_k[k-1]|^2} \tag{5a}$$

$$q_2[N] = q_2[0] - 2i\sum_{k=1}^{N}(\lambda_k - \lambda_k^*)\frac{\varphi_k^*[k-1]\psi_k[k-1]}{|\phi_k[k-1]|^2 + |\varphi_k[k-1]|^2 + |\chi_k[k-1]|^2 + |\psi_k[k-1]|^2} \tag{5b}$$

$$q_3[N] = q_3[0] - 2i\sum_{k=1}^{N}(\lambda_k - \lambda_k^*)\frac{\varphi_k^*[k-1]\chi_k[k-1]}{|\phi_k[k-1]|^2 + |\varphi_k[k-1]|^2 + |\chi_k[k-1]|^2 + |\psi_k[k-1]|^2} \tag{5c}$$

where

$$T[k] = \lambda_{k+1}I - H[k-1]A_kH[k-1]^{-1},$$

$$\Phi_k[k-1] = (T[k-1]T[k-2]\cdots T[1])|_{\lambda=\lambda_k}\Phi_k,$$

$$H[k-1]=\begin{pmatrix}\varphi_k[k-1] & \phi_k^*[k-1] & \psi_k^*[k-1] & \chi_k^*[k-1]\\ \phi_k[k-1] & -\varphi_k^*[k-1] & 0 & 0\\ \psi_k[k-1] & 0 & -\varphi_k^*[k-1] & 0\\ \chi_k[k-1] & 0 & 0 & -\varphi_k^*[k-1]\end{pmatrix},\ A_k=\begin{pmatrix}\lambda_k & 0 & 0 & 0\\ 0 & \lambda_k^* & 0 & 0\\ 0 & 0 & \lambda_k^* & 0\\ 0 & 0 & 0 & \lambda_k^*\end{pmatrix}.$$

Assume that $\Phi_1=(\varphi_1,\ \phi_1,\ \psi_1,\ \chi_1)=\Phi_1(\lambda_1,\ \eta)$ is a solution of equation (2) with $q_1=q_1[0]$, $q_2=q_2[0]$, $q_3=q_3[0]$ and $\lambda=\lambda_1+\eta$, η is a small parameter, then Φ_1 can be expanded as the Taylor series at $\eta=0$,

$$\Phi_1=\Phi_1^{[0]}+\Phi_1^{[1]}\eta+\Phi_1^{[2]}\eta^2+\cdots+\Phi_1^{[N]}\eta^N+\cdots \tag{6}$$

where $\Phi_1^{[k]}=(\varphi_1{}^{[k]},\ \phi_1{}^{[k]},\ \chi_1{}^{[k]},\ \psi_1{}^{[k]})^T$, $\Phi_1^{[k]}=\dfrac{1}{k!}\dfrac{\partial^k}{\partial\lambda^k}\Phi_1(\lambda)\Big|_{\lambda=\lambda_1}$, $(k=0,\ 1,\ 2,\cdots,N)$.

Then a generalized DT can be defined as:

$$\begin{aligned}\Phi_1[N-1]=&\Phi_1^{[0]}+\left[\sum_{l=1}^{N-1}T_1[l]\right]\Phi_1^{[1]}+\left[\sum_{l=1}^{N-1}\sum_{k>l}^{N-1}T_1[k]\,T_1[l]\right]\Phi_1^{[2]}+\cdots\\&+[T_1[N-1]\,T_1[N-2]\cdots T_1[1]]\Phi_1^{[N-1]},\end{aligned} \tag{7}$$

$$q_1[N]=q_1[0]-2i\sum_{k=1}^{N}(\lambda_1-\lambda_1^*)\frac{\varphi_k^*[k-1]\phi_k[k-1]}{|\phi_k[k-1]|^2+|\varphi_k[k-1]|^2+|\chi_k[k-1]|^2+|\psi_k[k-1]|^2}, \tag{8a}$$

$$q_2[N]=q_2[0]-2i\sum_{k=1}^{N}(\lambda_1-\lambda_1^*)\frac{\varphi_k^*[k-1]\psi_k[k-1]}{|\phi_k[k-1]|^2+|\varphi_k[k-1]|^2+|\chi_k[k-1]|^2+|\psi_k[k-1]|^2}, \tag{8b}$$

$$q_3[N]=q_3[0]-2i\sum_{k=1}^{N}(\lambda_1-\lambda_1^*)\frac{\varphi_k^*[k-1]\chi_k[k-1]}{|\phi_k[k-1]|^2+|\varphi_k[k-1]|^2+|\chi_k[k-1]|^2+|\psi_k[k-1]|^2}, \tag{8c}$$

where

$$T_1[k]=\lambda_1 I-H_1[k-1]\,A_1H_1[k-1]^{-1},$$

$$\Phi_1[N-1]=(\varphi_1[N-1],\ \phi_1[N-1],\ \psi_1[N-1],\ \chi_1[N-1])^T,$$

$$H_1[k-1]=\begin{pmatrix}\varphi_1[k-1] & \phi_1^*[k-1] & \psi_1^*[k-1] & \chi_1^*[k-1]\\ \phi_1[k-1] & -\varphi_1^*[k-1] & 0 & 0\\ \psi_1[k-1] & 0 & -\varphi_1^*[k-1] & 0\\ \chi_1[k-1] & 0 & 0 & -\varphi_1^*[k-1]\end{pmatrix},\ A_1=\begin{pmatrix}\lambda_1 & 0 & 0 & 0\\ 0 & \lambda_1^* & 0 & 0\\ 0 & 0 & \lambda_1^* & 0\\ 0 & 0 & 0 & \lambda_1^*\end{pmatrix}$$

3. Dynamics of localized waves

In order to construct localized wave solution on the bright–dark soliton background, the plane wave solution is considered as a seed solution. According to equation (1), such a seed solution can be obtained:

$$q_k[0]=d_ke^{i\theta}(k=1,\ 2,\ 3),\ \ \theta=(d_1+d_2+d_3)t \tag{9}$$

where d_k are the arbitrary constants. The special vector solution of Lax pair of equation (1) with $q_1[0]$, $q_2[0]$ and $q_3[0]$ at λ can be written as:

$$\Phi_1(\eta)=\begin{pmatrix}(C_1e^{M_1+M_2}-C_2e^{M_1-M_2})e^{-\frac{i\theta}{2}}\\ \rho_1(C_1e^{M_1-M_2}-C_2e^{M_1+M_2})e^{\frac{i\theta}{2}}+\alpha d_3e^{M_3}\\ \rho_2(C_1e^{M_1-M_2}-C_2e^{M_1+M_2})e^{\frac{i\theta}{2}}+\beta d_3e^{M_3}\\ \rho_3(C_1e^{M_1-M_2}-C_2e^{M_1+M_2})e^{\frac{i\theta}{2}}-(\alpha d_1+\beta d_2)e^{M_3}\end{pmatrix},$$

where

$$C_1=\frac{(\lambda+\sqrt{\lambda^2+(d_1^2+d_2^2+d_3^2)})^{\frac{1}{2}}}{\sqrt{\lambda^2+(d_1^2+d_2^2+d_3^2)}},\quad C_2=\frac{(\lambda-\sqrt{\lambda^2+(d_1^2+d_2^2+d_3^2)})^{\frac{1}{2}}}{\sqrt{\lambda^2+(d_1^2+d_2^2+d_3^2)}},$$

$$\rho_1=\frac{d_1}{\sqrt{d_1^2+d_2^2+d_3^2}},\ \rho_2=\frac{d_2}{\sqrt{d_1^2+d_2^2+d_3^2}},\ \rho_3=\frac{d_3}{\sqrt{d_1^2+d_2^2+d_3^2}},$$

$$M_1 = 0,\ M_2 = i\sqrt{\lambda^2 + (d_1^2 + d_2^2 + d_3^2)}\,(x + \lambda t + \Omega(\eta))$$

$$M_3 = -i\lambda(x + \lambda t),\ \Omega(\eta) = \sum_{k=1}^{N} s_k \eta^{2k},\ s_k = m_k + i n_k,\ (k = 1, 2, \cdots, N)$$

Here α, β, m_k, n_k are the arbitrary constants. Let $\lambda = i\sqrt{(d_1^2 + d_2^2 + d_3^2)}\ (1 + \eta^2)$ with a small parameter η, the vector function $\Phi_1(\eta)$ can expanded as Taylor series at $\eta = 0$

$$\Phi_1(\eta) = \Phi_1^{[0]} + \Phi_1^{[1]}\eta^2 + \Phi_1^{[2]}\eta^4 + \Phi_1^{[3]}\eta^6 + \cdots \tag{10}$$

where $\Phi_1^{[k]}$ can be obtained with Maple, and

$$\varphi_1{}^{[0]} = \frac{e^{-\frac{i\delta t}{2}}\sqrt{i\sqrt{\delta}}\,(2i\sqrt{\delta}x - 2\delta t - i)}{\delta}$$

$$\phi_1{}^{[0]} = \frac{\alpha d_3\,\delta\, e^{\sqrt{\delta}x + i\delta t} - 2d_1\left(i\sqrt{\delta}x - \delta t + \frac{i}{2}\right)e^{\frac{i\delta t}{2}}\sqrt{i\sqrt{\delta}}}{\delta}$$

$$\psi_1{}^{[0]} = \frac{\beta d_3\,\delta\, e^{\sqrt{\delta}x + i\delta t} - 2d_2\left(i\sqrt{\delta}x - \delta t + \frac{i}{2}\right)e^{\frac{i\delta t}{2}}\sqrt{i\sqrt{\delta}}}{\delta},$$

$$\chi_1{}^{[0]} = \frac{-(\alpha d_1 + \beta d_2)\delta\, e^{\sqrt{\delta}x + i\delta t} - 2d_3\left(i\sqrt{\delta}x - \delta t + \frac{i}{2}\right)e^{\frac{i\delta t}{2}}\sqrt{i\sqrt{\delta}}}{\delta},$$

with $\delta = d_1^2 + d_2^2 + d_3^2$. Moreover, the expressions of $\varphi_1{}^{[0]}$, $\phi_1{}^{[0]}$, $\psi_1{}^{[0]}$ and $\chi_1{}^{[0]}$ are omitted due to their cumbersome forms.

It is easy to determine that $\Phi_1[0] = \Phi_1^{[0]}$ is a vector solution of equation (2) with $q_1 = q_1[0]$, $q_2 = q_2[0]$, $q_3 = q_3[0]$ and $\lambda = \lambda_1$. According to equations (6)–(10), the first-order localized wave solutions of equation (1) are derived:

$$q_1[1] = q_1[0] - 2i(\lambda_1 - \lambda_1^*)\frac{\varphi_1^*[0]\phi_1[0]}{|\phi_1[0]|^2 + |\varphi_1[0]|^2 + |\chi_1[0]|^2 + |\psi_1[0]|^2}, \tag{11a}$$

$$q_2[1] = q_2[0] - 2i(\lambda_1 - \lambda_1^*)\frac{\varphi_1^*[0]\psi_1[0]}{|\phi_1[0]|^2 + |\varphi_1[0]|^2 + |\chi_1[0]|^2 + |\psi_1[0]|^2}, \tag{11b}$$

$$q_3[1] = q_3[0] - 2i(\lambda_1 - \lambda_1^*)\frac{\varphi_1^*[0]\chi_1[0]}{|\phi_1[0]|^2 + |\varphi_1[0]|^2 + |\chi_1[0]|^2 + |\psi_1[0]|^2}, \tag{11c}$$

Equation (11) involves free parameters d_1, d_2, d_3, α, β. With the change of those free parameters, the dynamics of the first-order localized wave solutions are discussed through the following three cases.

(1) $d_1 = d_2 = d_3 = 1$, $\alpha = 0$, $\beta = 0$.The components q_1, q_2 and q_3 are represented by the first-order rogue waves, which is similar to the case of standard NLS equation.

(2) $d_1 = 0$, $d_2 = 0$, $d_3 = 1$, $\alpha \neq 0$, $\beta \neq 0$. The first-order rogue wave on a bright- bright-dark soliton background can be derived. The interaction between a first-order rouge wave and a bright- bright-dark soliton is exhibited in figure 1. A rogue wave suddenly appears from nowhere at time t = 0, and these two waves superimpose with each other, The rogue wave cannot be easily identified at the zero-amplitude background, as shown in figures 1(a) and (b). It soon disappears afterwards, and the soliton continues moving forward. Moreover, the rogue wave moves far away from the soliton as the value of α and β, increases in figure 1.

(3) $d_1 = 0.5$, $d_2 = 0.5$, $d_3 = -1$, $\alpha \neq 0$, $\beta \neq 0$. The first-order rogue wave on a breather (Kuznetsov-Ma breather) background is presented in figure 2. The propagation direction of a breather is parallel to the positive direction of the t-axis, and a rogue wave suddenly appears at t = 0. It is observed that the breather and rogue waves merge as the value of α and β, increases.

Next, considering the following limit:

$$\Phi_1[1] = \lim_{\eta\to 0}\frac{T[1]|_{\lambda=\lambda_1(1+\eta^2)}\Phi_1}{\eta^2} = \lim_{\eta\to 0}\frac{(\lambda_1\eta^2 + T_1[1])\Phi_1}{\eta^2} = \lambda_1\Phi_1^{[0]} + T_1[1]\Phi_1^{[1]}, \tag{12}$$

where

$$T_1[1] = \lambda_1 I - H_1[0]A_1H_1[0]^{-1},\ \Phi_1^{[1]} = (\varphi_1^{[1]}, \phi_1^{[1]}, \psi_1^{[1]}, \chi_1^{[1]})$$

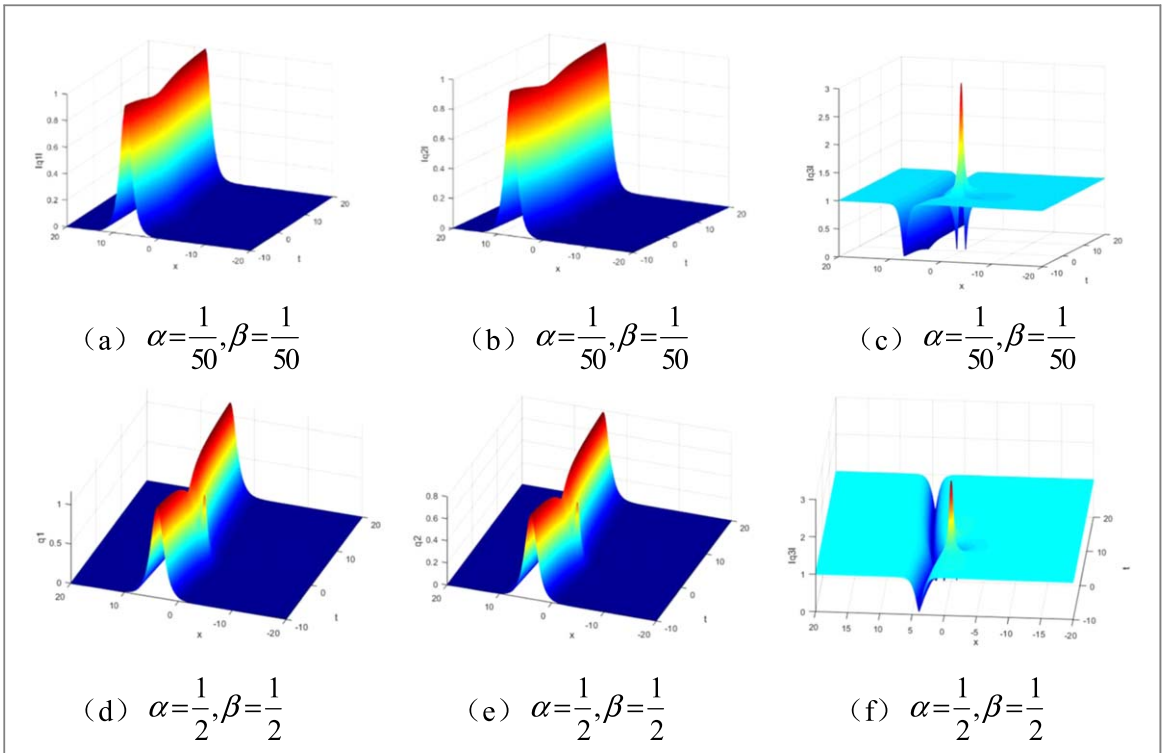

Figure 1. Evolution of the first-order bright-dark-rouge wave with parameters d1=0, d2=0, d3=1.

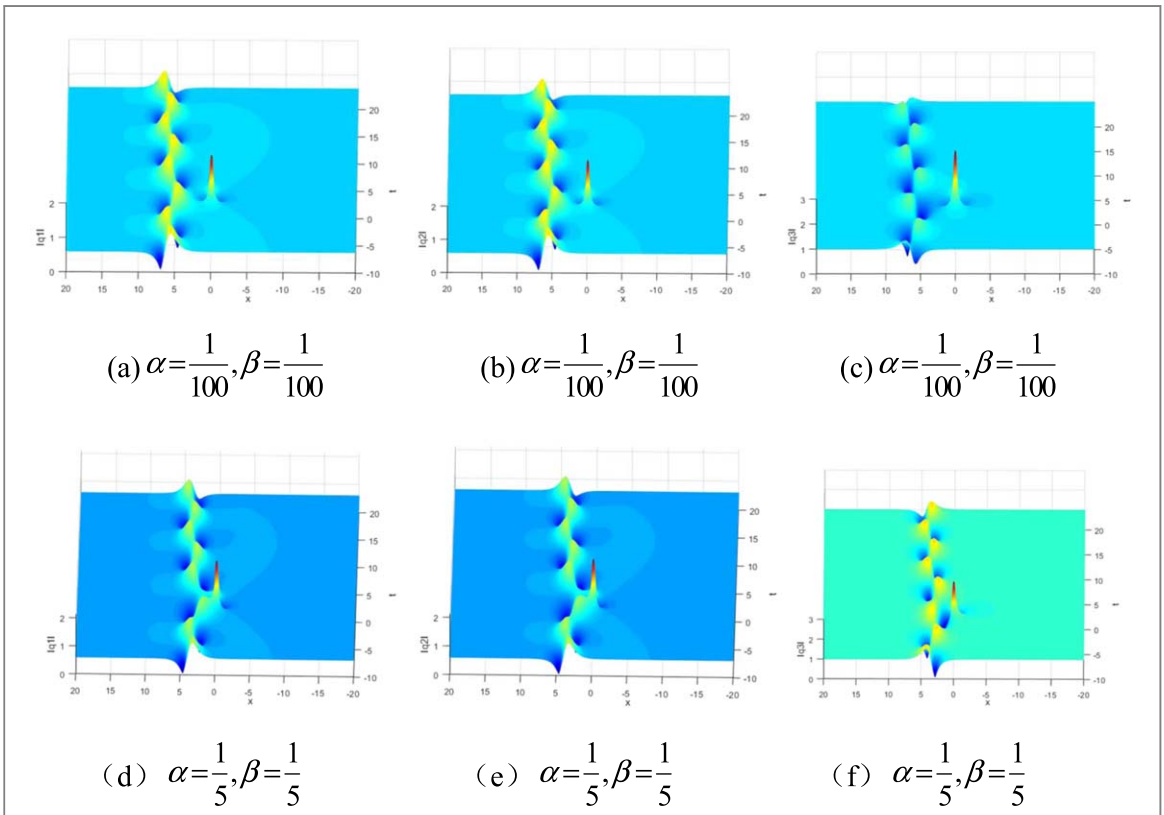

Figure 2. Evolution of the first-order KM breather-rouge wave with parameters $d_1 = 0.5$, $d_2 = 0.5$, $d_3 = -1$.

According to equations (6)–(12), the second-order localized wave solutions of equation (1) are obtained with the free parameters d_1, d_2, d_3, α, β, m_1, n_1,

$$q_1[2] = q_1[1] - 2i(\lambda_1 - \lambda_1^*)\frac{\varphi_1^*[1]\phi_1[1]}{|\phi_1[1]|^2 + |\varphi_1[1]|^2 + |\chi_1[1]|^2 + |\psi_1[1]|^2}, \tag{13a}$$

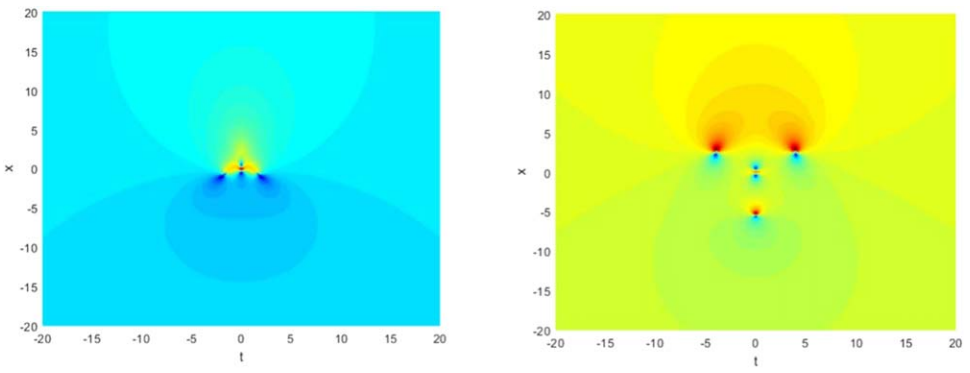

Figure 3. Evolution of the second-order rouge wave with parameters $d_1 = 0.5$, $d_2 = 0.5$, $d_3 = 1$, $\alpha = 0$, $\beta = 0$.

$$q_2[2] = q_2[1] - 2i(\lambda_1 - \lambda_1^*)\frac{\varphi_1^*[1]\psi_1[1]}{|\phi_1[1]|^2 + |\varphi_1[1]|^2 + |\chi_1[1]|^2 + |\psi_1[1]|^2}, \tag{13b}$$

$$q_3[2] = q_3[1] - 2i(\lambda_1 - \lambda_1^*)\frac{\varphi_1^*[1]\chi_1[1]}{|\phi_1[1]|^2 + |\varphi_1[1]|^2 + |\chi_1[1]|^2 + |\psi_1[1]|^2}, \tag{13c}$$

Similarly, the dynamical properties of the second-order localized wave solutions with the variations of the free parameters involved are discussed in the following cases:

1) $d_1 = 1$, $d_2 = 1$, $d_3 = 1$, $\alpha = 0$, $\beta = 0$. The contour plots of components q_1, q_2 and q_3 is shown in figure 3. Let $m_1 = n_1 = 0$, q_1, q_2 and q_3 are the second-order rogue wave, which is symmetric about $t = 0$, as shown in figure 3(a); For $m_1 = n_1 = 100$, a second-order rogue wave is separated into four first-order rogue waves and also symmetric distribution with respect to $t = 0$. The rogue wave has one hump and two valleys in the center, while the other three rogue waves, which have one hump and one valley, form a triangle around the center, as displayed in figure 3(b).

2) $d_1 = 0$, $d_2 = 0$, $d_3 = 1$, $\alpha \neq 0$, $\beta \neq 0$. Figure 4 shows a second-order rogue wave coexisting with two bright-dark solitons. The components q_1 and q_2 have similar structure, as exhibited in figures 4(a) and (b). In particular, the component q_3 has the one dark-soliton and a second-order rogue wave, as shown in figure 4(c). has a one-dark-soliton and a second-order rogue wave, as shown in figure 4(c). The second-order rogue wave separates from two dark-bright solitons by decreasing the value of α and β.

3) $d_1 = 0.5$, $d_2 = 0.5$, $d_3 = 1$, $\alpha \neq 0$, $\beta \neq 0$. The coexistence of a second-order rogue wave and two parallel breathers can be observed. While in component q_3, the two parallel Kuznetsov-Ma breathers don't travel in the same plane. As the value of α and β decreases, the second-order rogue wave and breathers separate, as shown in figure 5.

Further, consider the following limit:

$$\begin{aligned}\Phi_1[2] &= \lim_{\eta\to 0}\frac{T[2]|_{\lambda=\lambda_1(1+\eta^2)}T[1]|_{\lambda=\lambda_1(1+\eta^2)}\Phi_1}{\eta^4}\\ &=\lim_{\eta\to 0}\frac{(\lambda_1^2\eta^4 + \lambda_1(T_1[2] + T_1[1])\eta^2 + T_1[2]T_1[1])\Phi_1}{\eta^4}\\ &=\lambda_1^2\Phi_1^{[0]} + \lambda_1(T_1[2] + T_1[1])\Phi_1^{[1]} + T_1[2]T_1[1]\Phi_1^{[2]},\end{aligned} \tag{14}$$

where

$$T_1[1] = \lambda_1 I - H_1[0]A_1H_1[0]^{-1},\ \ T_1[2] = \lambda_1 I - H_1[1]A_1H_1[1]^{-1}$$

$$\Phi_1^{[1]} = (\varphi_1^{[1]}, \phi_1^{[1]}, \psi_1^{[1]}, \chi_1^{[1]}),\ \Phi_1^{[2]} = (\varphi_1^{[2]}, \phi_1^{[2]}, \psi_1^{[2]}, \chi_1^{[2]})$$

According to equations (6)–(14), the third-order localized wave solutions of equation (1) are obtained with the free parameters d_1, d_2, d_3, α, β, m_1, m_2, n_1, n_2,

$$q_1[3] = q_1[2] - 2i(\lambda_1 - \lambda_1^*)\frac{\varphi_1^*[2]\phi_1[2]}{|\phi_1[2]|^2 + |\varphi_1[2]|^2 + |\chi_1[2]|^2 + |\psi_1[2]|^2} \tag{15a}$$

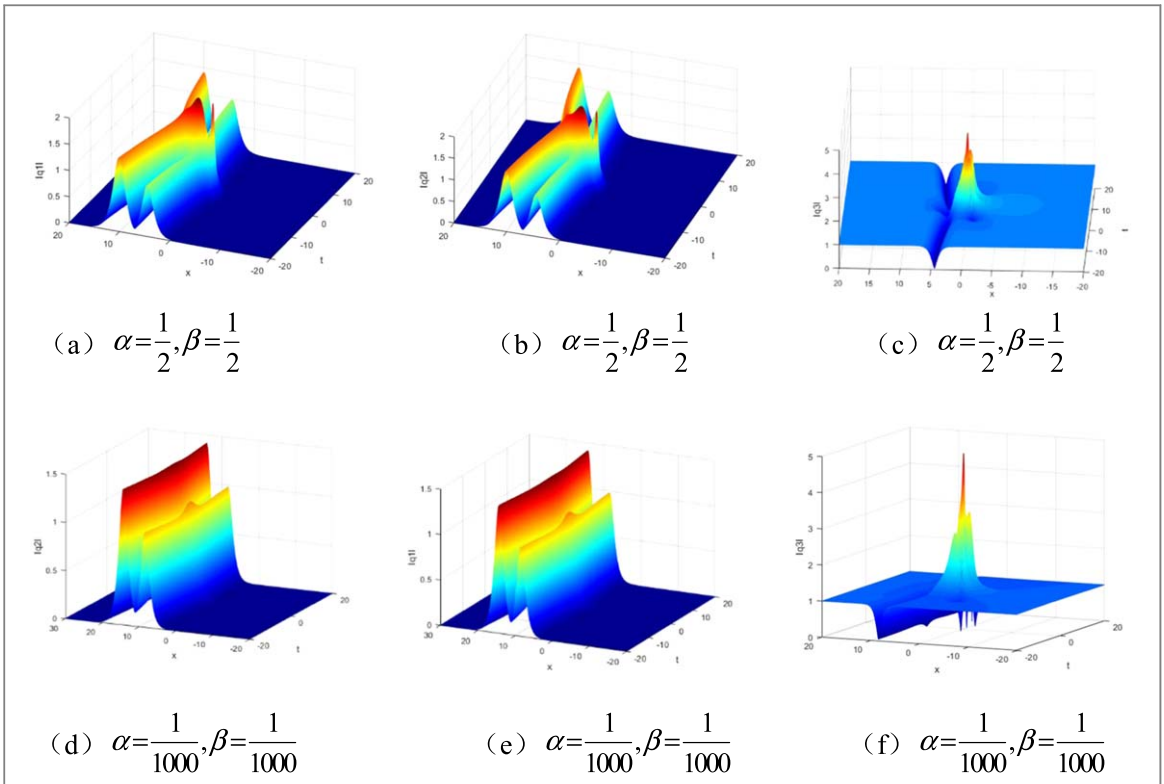

Figure 4. Evolution of the second-order bright-dark-rouge wave with parameters $d_1 = 0$, $d_2 = 0$, $d_3 = 1$, $m_1 = 0$, $n_1 = 0$.

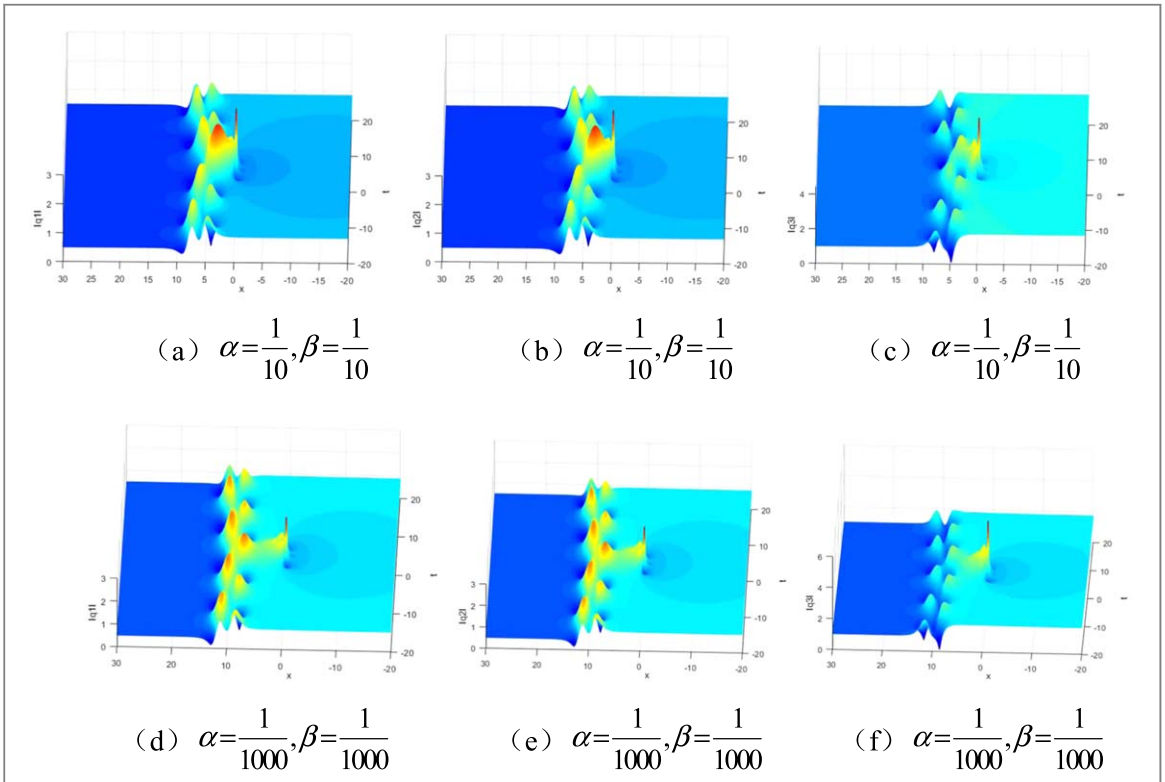

Figure 5. Evolution of the second-order KM breather-rouge wave with parameters $d_1 = 0.5$, $d_2 = 0.5$, $d_3 = 1$, $m_1 = 0$, $n_1 = 0$.

$$q_2[3] = q_2[2] - 2i(\lambda_1 - \lambda_1^*)\frac{\varphi_1^*[2]\psi_1[2]}{|\phi_1[2]|^2 + |\varphi_1[2]|^2 + |\chi_1[2]|^2 + |\psi_1[2]|^2} \tag{15b}$$

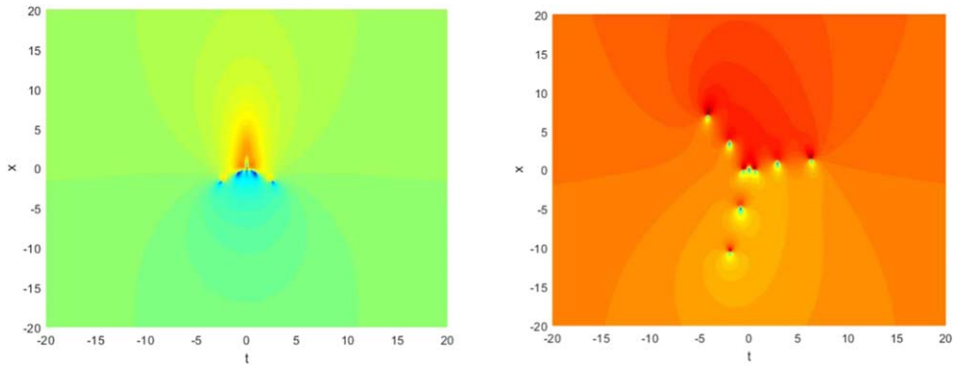

Figure 6. Evolution of the third-order rouge wave with parameters $d_1 = 1$, $d_2 = 1$, $d_3 = 1$, $\alpha = 0$, $\beta = 0$.

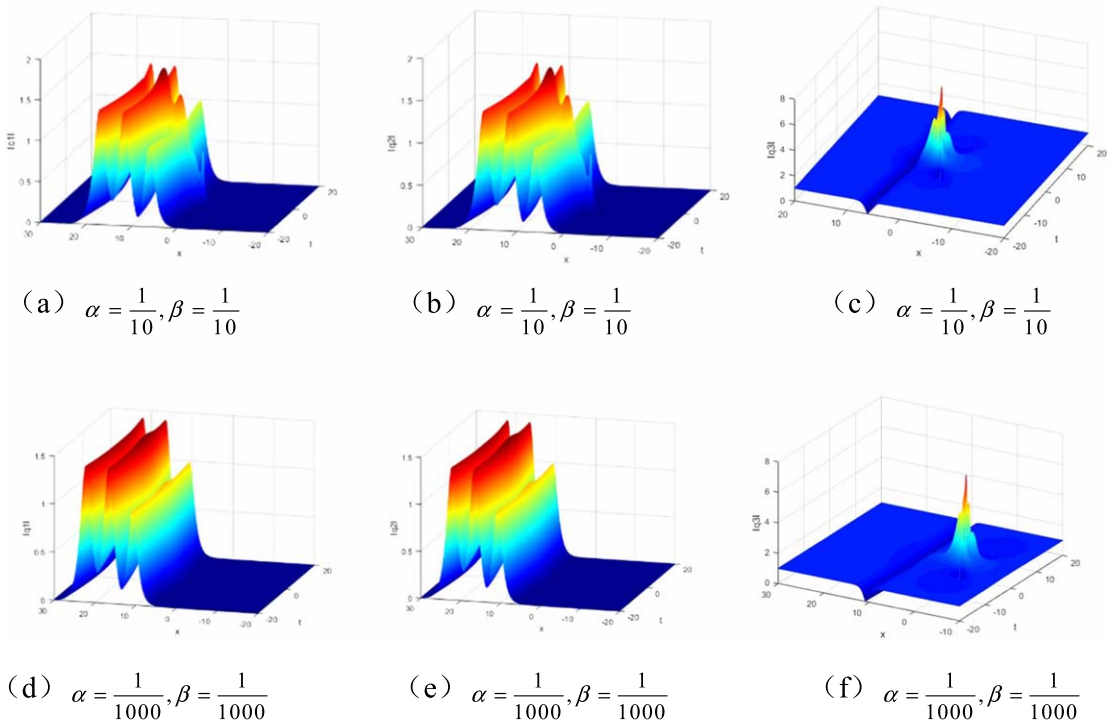

Figure 7. Evolution of the third-order bright-dark-rouge wave with parameters $d_1 = 0$, $d_2 = 0$, $d_3 = 1$, $m_1 = n_1 = m_2 = n_2 = 0$.

$$q_3[3] = q_3[2] - 2i(\lambda_1 - \lambda_1^*)\frac{\varphi_1^*[2]\chi_1[2]}{|\phi_1[2]|^2 + |\varphi_1[2]|^2 + |\chi_1[2]|^2 + |\psi_1[2]|^2} \tag{15c}$$

By taking different value of free parameters d_1, d_2, d_3, α, β, m_1, m_2, n_1, n_2, the dynamical behaviors of the third-order rogue waves on a multi-bright-dark soliton or multi-breather background are discussed in the following cases:

(1) $d_1 = d_2 = d_3 = 1$, $\alpha = 0$, $\beta = 0$.The contour plots of components q_1, q_2 and q_3 are shown in figure 6. Let $m_1 = n_1 = m_2 = n_2 = 0$, q_1, q_2 and q_3 are a third-order rogue wave and it is shaped like a flame, as shown in figure 6(a); For $m_1 = n_1 = m_2 = n_2 = 100$, a third-order rogue wave is separated into seven first-order rogue waves, the rogue wave which has one hump and two valleys is in the center, while the other six rogue waves are spread around in pairs, and the whole distribution is 'Y', as shown in figure 6(b).

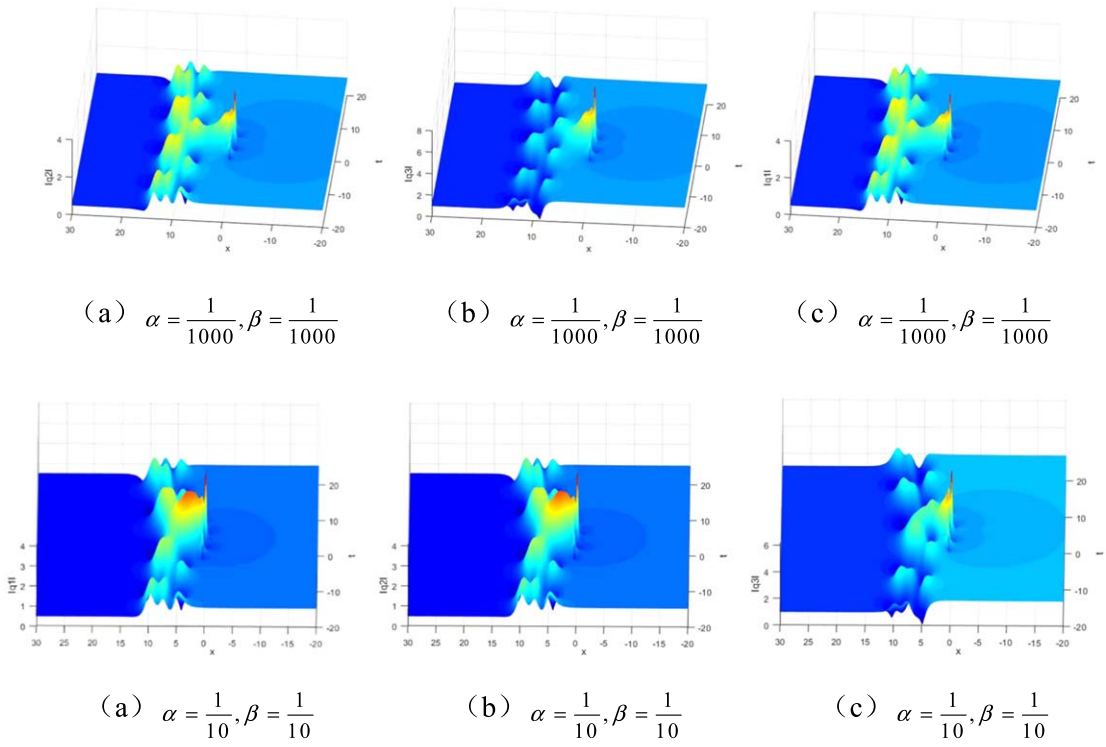

Figure 8. Evolution of the third-order breather-rouge wave with parameters $d_1 = 0.5$, $d_2 = 0.5$, $d_3 = 1$, $m_1 = n_1 = m_2 = n_2 = 0$.

(2) $d_1 = 0$, $d_2 = 0$, $d_3 = 1$, $\alpha \neq 0$, $\beta \neq 0$. Figure 7 displays a third-order rogue wave merged with three bright-dark solitons. Nevertheless, the component q_3 has a one dark-soliton and a third-order rogue wave. Moreover, the third-order rogue wave separates from two dark-bright solitons by decreasing the value of α and β.

(3) $d_1 = 0.5$, $d_2 = 0.5$, $d_3 = 1$, $\alpha \neq 0$, $\beta \neq 0$. The interaction between a third-order rogue wave and three breathers is demonstrated in figure 8. It is found that the propagation directions of three Kuznetsov-Ma breathers are parallel with the positive direction of t-axis, but the amplitude of breathers are inequality in component q_3. when the value of α and β increases, the rogue waves are farther away from the breathers.

4. Conclusions

This paper studies dynamical properties of solutions to the three-component coupled nonlinear Schrödinger equation. Based on a seed solution and a Lax pair, the iterative expressions of solutions to the equation are obtained by using a generalized DT. There are several parameters d_1, d_2, d_3, α, β, m_j and $n_j (j = 1, 2, 3 \cdots)$ that play an important role in the interaction dynamics among different nonlinear waves. By choosing different values of those free parameters, the rogue waves on constant, multi-bright-dark soliton and multi-breather backgrounds are obtained, and the corresponding evolution plots are provided. Moreover, the rogue waves are farther away from the soliton or breather as the parameters α and β, are decreased. The results of this paper exhibit rich dynamics of three-component coupled nonlinear systems.

Acknowledgments

The authors sincerely thanks for the support of the National Natural Science Foundation of China (NNSFC) through grant No.11602232, Research Project Supported by Shanxi Scholarship Council of China through grant No.2022–150 and Natural Science Foundation of Shanxi Province through grant No.202203021211086 and No.202203021211088.

Data availability statement

No new data were created or analysed in this study.

ORCID iDs

N Song https://orcid.org/0000-0002-0629-7015
W X Ma https://orcid.org/0000-0001-5309-1493

References

[1] Mu G, Qin Z Y and Grimshaw R 2015 Dynamics of rogue waves on a multi-soliton background in a vector nonlinear Schrödinger equation *SIAM J. Appl. Math.* **75** 1–20
[2] Guo B L and Ling L M 2011 Rogue wave, breathers and bright-dark-rogue solutions for the coupled Schrödinger equations *Chin. Phys. Lett.* **28** 110202
[3] Baronio F *et al* 2012 Solutions of the vector nonlinear schrödinger equations: evidence for deterministic rogue waves *Phys. Rev. Lett.* **109** 044102
[4] Wang X *et al* 2014 Higher-order localized waves in coupled nonlinear schrödinger equations *Chin. Phys. Lett.* **31** 090201
[5] Zhao L C and Liu J 2013 Rogue-wave solutions of a three-component coupled nonlinear Schrödinger equation *Phys. Rev. E* **87** 013201
[6] Feng B F 2014 General N-soliton solution to a vector nonlinear Schrödinger equation *Journal of Mathematical and Theoretical* **47** 355203
[7] Ma W X and Batwa S 2021 A binary darboux transformation for multicomponent NLS equations and their reductions *Analysis and Mathematical Physics* **11** 44
[8] Zhang G Q and Yan Z Y 2018 Three-component nonlinear Schrödinger equations: modulational instability, N th-order vector rational and semi-rational rogue waves, and dynamics *Commun. Nonlinear Sci. Numer. Simul.* **62** 117–33
[9] Gao X Y, Guo Y J and Shan W R 2020 Shallow water in an open sea or a wide channel: auto- and non-auto- Bäcklund transformations with solitons for a generalized (2 + 1)-dimensional dispersive long-wave system *Chaos Solitons Fractals* **138** 109950
[10] Gao X Y, Guo Y J and Shan W R 2020 Water-wave symbolic computation for the earth, enceladus and titan: the higher-order boussinesq–burgers system, auto and non-auto- Bäcklund transformations *Appl. Math. Lett.* **104** 106170
[11] Chen Y Q *et al* 2020 Ablowitz–Kaup–Newell–Segur system, conservation laws and Bcklund transformation of a variable-coefficient Korteweg–de Vries equation in plasma physics, fluid dynamics or atmospheric science *Int. J. Mod. Phys. B* **34** 2050226
[12] Ma W X 2020 Long-time asymptotics of a three-component coupled nonlinear Schrödinger system *J. Geom. Phys.* **153** 103669
[13] Deift P and Zhou X 1993 A steepest descent method for oscillatory riemann–hilbert problems. asymptotics for the MKdV equation *Ann. Math.* **137** 295–368
[14] Geng X G and Liu H 2018 The nonlinear steepest descent method to long-time asymptotics of the coupled nonlinear Schrödinger equation *Journal of Nonlinear Science* **28** 739–63
[15] Geng X G, Wang K D and Chen M M 2021 Long-time asymptotics for the spin-1 Gross–Pitaevskii equation *Commun. Math. Phys.* **382** 581–611
[16] Ma W X 2019 Application of the riemann–hilbert approach to the multicomponent AKNS integrable hierarchies *Nonlinear Anal. Real World Appl.* **47** 1–17
[17] Matveev V B and Salle M A 1991 Darboux transformations and solitons. springer series in nonliner *Dynamics* (New York, Berlin: Springer-Verlag)
[18] Gu C H, Hu H S and Darboux Z X Z 2005 *Transformations in Integrable Systems* (New York, Berlin: Springer-Verlag)
[19] Cieliński J L 2009 Algebraic construction of the Darboux matrix revisited *J. Phys. A: Math. Theor.* **42** 404003
[20] Zhang C R, Tian B, Qu Q X, Liu L and Tian H Y 2020 Vector bright solitons and their interactions of the couple Fokas–Lenells system in a birefringent optical fiber *Journal of Applied Mathematics and Physics* **71** 18
[21] Du Z, Tian B, Qu Q X and Zhao X H 2020 Characteristics of higher-order vector rogue waves to a coupled fourth-order nonlinear Schrödinger system in a two-mode optical fiber *The European Physical Journal Plus* **135** 241
[22] Geng X G, Li R M and Xue B 2020 A vector general nonlinear schrödinger equation with m + n components *Journal of Nonlinear Science* **30** 991–1013
[23] Kanna T and Lakshmanan M 2001 Exact soliton solutions, shape changing collisions, and partially coherent solitons in coupled nonlinear Schrödinger equations *Phys. Rev. Lett.* **86** 5043–6
[24] Baronio F, Degasperis A, Conforti M and Wabnitz S 2012 Solutions of the vector nonlinear Schrödinger equations: evidence for deterministic rogue waves *Phys. Rev. Lett.* **109** 044102
[25] Rogister A 1971 Parallel propagation of nonlinear low-frequency waves in high-β plasma *The Physics of Fluids* **14** 2733–9
[26] Ablowitz M J, Prinari B and Trubatch A D 2004 *Discrete and Continuous Nonlinear Schrödinger Systems* (Cambridge: Cambridge University Press)
[27] Dalfovo F, Giorgini S, Pitaevskii L P and Stringari S 1999 Theory of bose–einstein condensation in trapped gases *Review of Modern Physics* **71** 463–512
[28] Vijayajayanthi M, Kanna T and Lakshmanan M 2009 Multisoliton solutions and energy sharing collisions in coupled nonlinear Schrödinger equations with focusing, defocusing and mixed type nonlinearities *Eur. Phys. J. Spec. Top.* **73** 57–80
[29] Zhang G Q and Yan Z Y 2018 Three-component nonlinear Schrödinger equations: Modulational instability, Nth-order vector rational and semi-rational rogue waves, and dynamics *Commun. Nonlinear Sci. Numer. Simul.* **62** 117–33
[30] Xiu B, Wang B *et al* 2019 The three-component coupled nonlinear Schrödinger equation: Rogue waves on a multi-soliton background and dynamics *Europhys. Lett.* **126** 15001
[31] Peng W Q *et al* 2019 Riemann-hilbert method and multi-soliton solutions for three-component coupled nonlinear Schrödinger equations *J. Geom. Phys.* **146** 103508